Journal of Materials Chemistry C

PAPER

View Article Online
View Journal | View Issue

Cite this: J. Mater. Chem. C, 2018, 6, 4777

Enhanced NIR-I emission from water-dispersible NIR-II dye-sensitized core/active shell upconverting nanoparticles†

Chanchal Hazra,*[a] Sajjad Ullah,[ab] York E. Serge Correales,[a] Laís G. Caetano[a] and Sidney J. L. Ribeiro*[a]

Recently, there has been a surge in research studies directed towards near-infrared (NIR) dye-sensitized upconverting nanoparticles (UCNPs) as they carry the prominent advantages of a broader absorption range and enhanced upconversion efficiency. Unfortunately, however, the UCNPs combined with the native form of NIR dye are of little use for biological imaging in the NIR-I or NIR-II window as the dye-sensitization process is mostly carried out in non-aqueous media. To overcome this shortcoming, we propose to employ a water-dispersible NIR-II dye (IR-1061) to sensitize core/active shell UCNPs and achieve sufficiently high upconversion quantum efficiency in aqueous media. We have particularly focused on achieving strong NIR-I emission rather than visible upconversion emission as the latter suffers from the problem of shallow tissue penetration depth. For this purpose, Pluronic F68-encapsulated water-dispersible IR-1061 dye was coupled with polyethyleneimine (PEI)-coated $NaYF_4:Tm^{3+}/Yb^{3+}@NaYF_4:Yb^{3+}$ core/active shell UCNPs. We thus achieved a 283% enhancement in NIR-I emission (*i.e.* 800 nm emission of Tm^{3+} ion) from water-dispersible NIR-II dye-sensitized core/active shell UCNPs *via* doping of ytterbium ions (Yb^{3+}) in the UCNP shell, which bridged the energy transfer from the dye to the UCNP core. Practically, in comparison with the native form of the dye, this water-dispersible dye can also efficiently harvest irradiation energy, which is nonradiatively transferred to Yb^{3+} ions in the shell and subsequently to Yb^{3+} ions in the core. The latter sensitizes Tm^{3+} ions positioned in the core, thus generating upconversion luminescence from the UCNPs. We envision that our water-dispersible NIR-II dye-sensitized core/active shell UCNPs are not only potential candidates for a broad spectrum of photonic applications but that they will also find new opportunities in several biological applications.

Received 20th January 2018,
Accepted 25th March 2018

DOI: 10.1039/c8tc00335a

rsc.li/materials-c

Introduction

In recent years, UCNPs, which possess the ability to convert low-energy radiation into high-energy photons *via* the multiphoton process, have been gaining enormous research attention.[1–11] This interest is mainly attributed to the growing importance of these UCNPs in areas such as bioimaging, biosensing, solar cells and volumetric displays, among others.[12–24] The UCNPs are generally composed of lanthanide (Ln^{3+}) ions that are spatially distributed in an appropriate host matrix.[25–27] The Ln^{3+} ions contribute interesting optical properties to UCNPs such as sharp luminescence signals and longer luminescence lifetimes (μs to ms) and even exhibit multiple emissions spanning a wide region (UV to NIR), which are exploited in a wide range of applications including phosphors, lasing, biomarkers, optoelectronic devices, to name a few.[28–31]

Some recent research attempts have enabled good control over UCNP size, phase and emission colours.[32–34] However, their emission brightness and excitation wavelength range are limited by the weak and narrow band absorption of lanthanide ions due to the parity-forbidden character of the intra-4f transition.[35,36] Recently, different strategies such as surface plasmon resonance effects from metal nanoparticles, optimal dopant concentration and formation of core/shell nanostructures have been employed to enhance upconversion luminescence from UCNPs.[37–43] Unfortunately, however, most of these strategies suffer from limitations such as low absorption coefficient, narrow excitation band and low absorption cross section of Yb^{3+} ions. For example, Yb^{3+} ions absorb light in a spectral window of ~938–975 nm, which is about 10 times narrower than that of organic dye molecules. Similarly, their absorption cross section

[a] Institute of Chemistry, São Paulo State University, UNESP, 14800-060, Araraquara, SP, Brazil. E-mail: sidney@iq.unesp.br, chanchalhazra007@gmail.com; Tel: +55-1633019631
[b] Institute of Chemical Sciences, University of Peshawar, 25120, Peshawar, Pakistan

† Electronic supplementary information (ESI) available: XRD, IR spectra, UC and DC spectra, TEM, UV, power dependence, zeta potential, energy transfer mechanism, photostability, overlap spectra, PL spectra. See DOI: 10.1039/c8tc00335a

is 1000 to 10 000 times lower than that of traditional organic dye molecules.[44,45] These fundamental features limit UCNPs in broadly harvesting near infrared (NIR) light and producing bright upconversion luminescence, thus restricting their scope of utility in a wide range of applications.

To address the problems of the low intensity absorption and narrow excitation band of Yb^{3+}-doped UCNPs and allow their use in clinical applications, researchers are still developing nanomaterials with high upconversion emission under low excitation power density. Following this trend, recently, a few reports suggested the use of NIR dyes to sensitize UCNPs to significantly improve their upconversion performance. In such cases, if the dominating NIR-emissive peaks of the dye overlap well with the absorption of sensitizer ions (*e.g.* Yb^{3+}, Nd^{3+}), a suitable combination of NIR dye and UCNPs with sensitizer ions (*e.g.* Yb^{3+}, Nd^{3+}) doped in the shell could afford superior upconversion luminescence upon NIR laser excitation. Concerning this issue, Hummelen's research group first designed and synthesized IR-806 dye conjugated $NaYF_4$:Er^{3+}/Yb^{3+} UCNPs and they observed a giant enhancement in the upconversion emission.[46] The shortcoming of their work was a large energy mismatch between Yb^{3+} ion and dye molecule leading to low energy transfer. In fact, the utilized UCNPs ($NaYF_4$:Yb^{3+}/Er^{3+}) had to be devoid of any shell in order to allow dye sensitization to occur efficiently. Moreover, strong surface-related deactivations manifested that typically led to upconversion luminescence quenching, two to three orders stronger than that for a core/shell structure with suppressed deactivation.[47] These limitations resulted in a very low upconversion quantum efficiency from the UCNPs. Later on, Prasad *et al.* introduced the cascade energy upconversion concept to mitigate such drawbacks and they also observed a large enhancement in visible upconversion emission as well as high energy transfer and high ($\sim$19%) quantum efficiency.[48] These excellent features allow the UCNPs to exhibit unrivalled three photon blue upconversion using a biocompatible 808 nm infrared light excitation with a power density comparable to that of solar irradiation at the earth surface. The same research group has shown the use of dye-sensitized UCNPs for multicolour emission bands in the NIR-II window, which seems more relevant over the NIR-I window for biological applications.[7] They demonstrated that the NIR-II emission from indocyanine green dye-sensitized Er^{3+}-doped $NaYF_4$:Yb^{3+}/X^{3+}@$NaYbF_4$@$NaYF_4$:Nd^{3+} (X = null, Er, Ho, Tm, Pr) core/shell/shell nanocrystals allows a sharp image through 9 mm thick chicken breast tissue. Not only that, the emission signal detection through 22 mm thick tissue yields a better imaging profile than from the typically used Yb^{3+}/Tm^{3+} co-doped UCNPs imaged in the NIR-I region (700–950 nm). Han and co-workers have applied dye-sensitized UCNPs for optogenetic analysis in the NIR tissue optical window for potential use in controlling neuronal activity.[49] In particular, using dye-sensitized core/active shell UCNPs embedded poly(methyl methacrylate) polymer implantable systems, they successfully shifted the optogenetic neuron excitation window to a biocompatible and deep tissue penetrable 800 nm wavelength. Very recently, Lin's research group has shown the use of dye-sensitized UCNPs for multimodal imaging applications *in vitro* and *in vivo*.[50] The use of dual photosensitizers and the upconverted visible emissions from $NaGdF_4$:Yb^{3+}/Er^{3+}@$NaGdF_4$:Nd^{3+}/Yb^{3+} core/shell UCNPs allow for the activation of photodynamic therapy (PDT) agents to generate reactive oxygen species for antitumor therapy.

However, most of the reports mentioned above are related to NIR-I dye in its native form and their particular focus was based on visible upconversion emission. To the best of our knowledge, there is no report available on water-dispersible NIR-II dye-sensitized core/active shell UCNPs. In this research study, we for the first time synthesized and used water-dispersible NIR-II dye (IR-1061) to carry out sensitization experiments in aqueous medium, which is biologically more important. Our main goal was to achieve a strong NIR-I (*e.g.* $\sim$800 nm emission from Tm^{3+} ion) signal, which is more beneficial for bioimaging applications over visible emission as the latter has shallow tissue penetration. More specifically, PEI-coated $NaYF_4$:Tm^{3+}/Yb^{3+}@$NaYF_4$:Yb^{3+} core/active shell UCNPs and Pluronic F68 encapsulated water-dispersible IR-1061 dye sensitization synergistically make the UCNPs promising to provide highly intense NIR-I signal under 980 nm laser excitation.

Experimental

Materials

Y_2O_3 (99.99%, Sigma-Aldrich), Yb_2O_3 (99.99%, Sigma-Aldrich), Tm_2O_3 (99.99%, Sigma-Aldrich), HCl (Synth), NaOH (Synth), NH_4F (Merck), methanol (CH_3OH, Synth), 1-octadecene (ODE, Aldrich), oleic acid (OA, Aldrich), cyclohexane (Synth, Brazil), ethanol (C_2H_5OH, Synth, Brazil), diethyl ether (Synth, Brazil), polyethyleneimine (PEI, Sigma-Aldrich, mol. wt. 800), Pluronic-F68 (Sigma), IR-1061 (Aldrich) and IR-806 (Aldrich) were used in this study. All chemicals were used without further purification.

Synthesis of β-$NaYF_4$:Yb^{3+}(30)/Tm^{3+}(0.5) core UCNPs.

The core $NaYF_4$:Yb^{3+}(30)/Tm^{3+}(0.5) UCNPs were synthesized following a modified co-precipitation method according to a literature report.[51] In a typical experiment, 4 mL of an aqueous solution (0.2 M) of $LnCl_3{\cdot}6H_2O$ (Ln = Y, Yb and Tm) was added to a 100 mL three-necked flask containing oleic acid (6 mL) and 1-octadecene (14 mL). The resulting mixture was heated to 150 °C and kept for 1.5 h to form lanthanide oleate complexes and then cooled down to 50 °C. Subsequently, a methanol solution (10 mL) containing NH_4F (3.25 mmol) and NaOH (2.0 mmol) was added and the mixture was stirred at 50 °C for 45 min. The temperature of the reaction mixture was then increased to 100 °C to remove methanol. Upon removal of the methanol and keeping the reaction mixture at 100 °C under vacuum, the solution was heated to 290 °C under a N_2 atmosphere and kept for 1.5 h before cooling down to room temperature naturally. The resulting nanoparticles were precipitated out by the addition of ethanol, collected by centrifugation, washed with cyclohexane, ethanol and methanol and finally redispersed in 4 mL of cyclohexane.

Synthesis of β-$NaYF_4$:Yb^{3+}(30)/Tm^{3+}(0.5)@$NaYF_4$:Yb^{3+}(*X*) (*X* = 0, 2, 5, 10, 20) core/active shell UCNPs

In a typical experiment, 4 mL of a solution (0.2 M) of $LnCl_3{\cdot}6H_2O$ (Ln = Y, Yb) in water was added to a 100 mL three-necked flask

containing oleic acid (6 mL) and 1-octadecene (14 mL). The mixture was then heated to 150 °C and kept for 1.5 h with magnetic stirring and then cooled down to 50 °C naturally. Afterwards, $NaYF_4$:Yb^{3+}/Tm^{3+} core UCNPs in 4 mL of cyclohexane were added along with a 10 mL methanol solution of NH_4F (3.25 mmol) and NaOH (2.0 mmol). The resulting mixture was stirred at 50 °C for 45 min. The temperature of the reaction mixture was heated to 100 °C to remove the methanol. Upon removal of the methanol and keeping the reaction mixture at 100 °C under vacuum, the solution was then heated to 290 °C under a N_2 atmosphere and kept for 1.5 h before cooling down to room temperature naturally. The resulting nanoparticles were precipitated out by the addition of ethanol, collected by centrifugation, washed with cyclohexane, ethanol and methanol and finally redispersed in 4 mL of cyclohexane.

Preparation of hydrophilic β-$NaYF_4$:Yb^{3+}(30)/Tm^{3+}(0.5)@ $NaYF_4$:Yb^{3+}(X) (X = 0, 2, 5, 10, 20) core/active shell UCNPs.

A total of 1.3 mL of a cyclohexane dispersion of the core/active shell UCNPs was precipitated by the addition of ethanol and redispersed in 5 mL of HCl solution (0.1 M in deionized water). The slurry was then sonicated and stirred for 1 h and 3 h, respectively, to remove the oleate ligands from the surface of the UCNPs. The aqueous solution was mixed with diethyl ether in a separating funnel to remove the oleic acid by extraction with diethyl ether. The aqueous portion containing the UCNPs was collected in a centrifuge tube. The UCNPs in the aqueous fraction were recovered by centrifugation after precipitation with acetone. This process was repeated twice and finally the UCNPs were dispersed in 10 mL of water. Then, the ligand-free core/active shell UCNP aqueous dispersion was mixed with PEI solution (10 mg mL^{-1}), followed by vigorous stirring for 12 h. PEI coated core/active shell UCNPs were obtained followed by centrifugation at 13 000 rpm for 30 min. The product was washed with distilled water by sonication and centrifugation twice. Finally, the PEI coated core/active shell UCNPs were dispersed in 4 mL of water for further use.

The preparation of water-dispersible IR-1061 dye and the water-dispersible IR-1061 dye-sensitized core and core/active shell UCNP dispersion in water is discussed in Section SA and Section SB of the ESI,† respectively.

Characterization

Fourier transform infrared (FTIR) spectra were collected using a PerkinElmer Spectrum 1000 FT-IR spectrometer with a resolution of 2 cm^{-1} and averaged over four scans. Room temperature optical absorption spectra of the samples were recorded on a Varian model Cary 5000 spectrophotometer. The samples were taken in a 3 mL quartz cuvette (path length, 2 cm). The XRD measurements were performed on a D8 Advance Powder X-ray diffractometer (Bruker) operated at 30 mA and 30 kV using Ni-filtered Cu Kα X-ray radiation (λ = 1.540 Å) at a scanning rate of 1° min^{-1} in the 2θ range from 10° to 70°. TEM analyses of the samples supported on holey carbon-coated copper grids were carried out using an FEI TECNAI (G^2F20) transmission electron microscope operated at an accelerating voltage of 200 kV. Upconversion emission spectra of the core and core/active shell UCNPs were acquired using a Horiba Jobin Yvon spectrofluorometer (model fluorolog-3 FL3-122) equipped with a photomultiplier tube (model R 928 P, Spex) sensitive between 250 and 850 nm. A 980 nm laser diode (from DMC, Brazil) coupled with an optical fiber (200 μm diameter) was utilized as the excitation source. All spectra were acquired in an identical fashion under the same experimental conditions and the upconversion emission measurements were carried out at an optical spectral resolution of 1 nm. The laser power used in the measurement was 7 W cm^{-2} and the beam diameter was 1 mm. The same experimental conditions were used to measure downshifting luminescence of the samples. The photoluminescence (PL) emission spectra were collected using a Jobin Yvon Fluorolog system under 980 nm diode laser excitation and the signal was detected using an NIR PMT module detector (HAMAMATSU, H10330A series). The emission lifetime measurements were performed with the Horiba Jobin Yvon Fluorolog-3 machine (USA); FL3-122 model; spectrometer equipped with a Xenon pulsed bulb with 0.15 Joules per flash. The dynamic light scattering (DLS) data were collected using a Malvern Zetasizer Nano equipped with a 4.0 mW He–Ne laser operating at 633 nm. All samples were measured in an aqueous system at room temperature with a scattering angle of 173°. The size distribution was calculated by Nano software and is derived from a non-negative least square (NNLS) analysis.

Results and discussion

The efficient energy transfer between Yb^{3+} and Tm^{3+} ions and upconversion emission in the core $NaYF_4$:Yb^{3+}(30)/Tm^{3+}(0.5) UCNPs is well reported and can be further enhanced through dye-sensitization and the proper choice of core/active shell configuration. In our strategy to obtain strong NIR-I upconversion emission along with high energy transfer upconversion, we coated the core $NaYF_4$:Yb^{3+}(30)/Tm^{3+}(0.5) particles with an active shell of $NaYF_4$:Yb^{3+} (X = 0, 2, 5, 10 and 20) and the resulting core/active shell UCNPs, after surface modification with PEI, were combined with a Pluronic F68 encapsulated, water-dispersible NIR-II (IR-1061) dye. Doping of ytterbium ions (Yb^{3+}) in the UCNP shell was used to bridge the energy transfer from the dye to the UCNP core (Scheme 1).

Phase analysis of the core and core/active shell UCNPs was performed using powder X-ray diffraction (PXRD) measurement (Fig. S1, ESI†). All diffraction peaks perfectly match with the standard diffraction pattern of hexagonal $NaYF_4$ crystals (JCPDS No. 28-1192).

The TEM images of oleic acid capped $NaYF_4$:Yb^{3+}(30)/Tm^{3+}(0.5)@ $NaYF_4$:Yb^{3+} (X = 0, 2, 5, 10, 20) core/active shell UCNPs along with their corresponding core particles are shown in Fig. 1 and Fig. S2 (ESI†). TEM images show the formation of uniform and monodisperse nanoparticles with an average diameter of 27 nm and 38 nm for the core and core/active shell UCNPs, respectively. The shell thickness of the core/active shell UCNPs is thus estimated to be around 5 nm. Monodispersity in the size of the core and core/active shell UCNPs is evident from the size distribution histograms shown in Fig. S3 (ESI†).

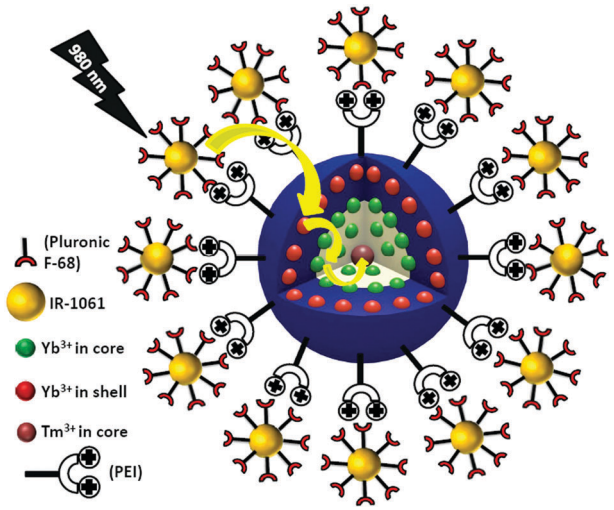

Scheme 1 Scheme illustrating energy transfer mechanism between Pluronic F68 encapsulated IR-1061 dye and PEI-coated core/active shell UCNPs, producing enhanced NIR-I upconversion emission from the activator (Tm^{3+}) positioned in the core.

The surface capping of core and core/active shell UCNPs with oleic acid is confirmed by the appearance of a strong carbonyl stretching vibration near 1710 cm^{-1} (*vide infra*). This frequency is much lower than that observed for the free oleic acid molecules.

The presence of Yb^{3+} ions in the core and core/active shell UCNPs is confirmed by the presence of their characteristic absorption peak in the electronic absorption spectra of the samples (Fig. S4, ESI†). The absorption intensity of this characteristic peak of Yb^{3+} ion increases with an increase in the Yb^{3+} concentration in the shell, suggesting efficient incorporation of Yb^{3+} ions in the shell.

Fig. 2 shows the upconversion emission spectra of the core and core/active shell UCNPs obtained under 980 nm laser excitation. Strong blue and NIR emissions are observed near 450, 477 and 800 nm, respectively. These emissions are ascribed to the $^1D_2 \rightarrow {}^3F_4$, $^1G_4 \rightarrow {}^3H_6$ and $^3H_4 \rightarrow {}^3H_6$ transitions of Tm^{3+}, respectively. In addition, other peaks observed near 359 and 650 nm are assigned to the transitions $^1D_2 \rightarrow {}^3H_4$ and $^1G_4 \rightarrow {}^3F_4$, respectively. These emissions originate from the excited energy levels of Tm^{3+} ions,

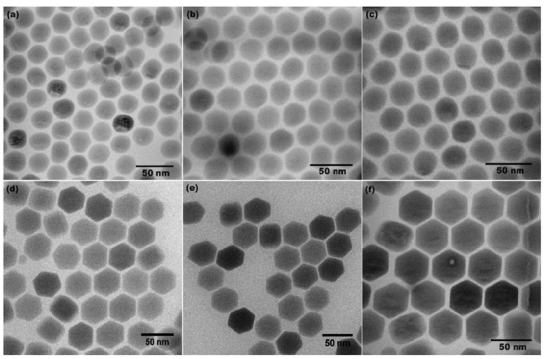

Fig. 1 TEM images of (a–c) oleic acid capped $NaYF_4$:$NaYF_4$:Yb^{3+}(30)/Tm^{3+}(0.5) core particles and (d–f) the corresponding $NaYF_4$:Yb^{3+}(30)/Tm^{3+}(0.5)@$NaYF_4$:Yb^{3+}(*X*) core/active shell UCNPs where *X* = 0, 5 and 10%, respectively.

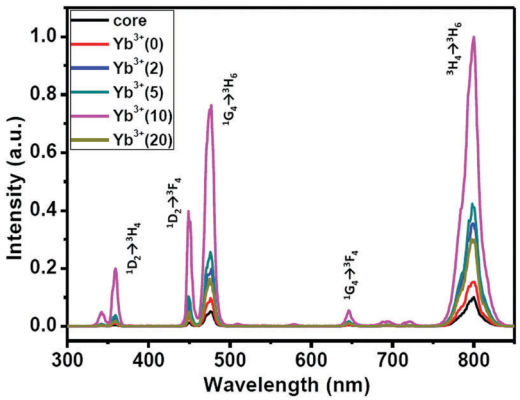

Fig. 2 Upconversion emission spectra of oleic acid capped $NaYF_4$:$NaYF_4$:Yb^{3+}(30)/Tm^{3+}(0.5) core particles and $NaYF_4$:$NaYF_4$:Yb^{3+}(30)/Tm^{3+}(0.5)@$NaYF_4$:Yb^{3+}(*X*) (*X* = 0, 2, 5, 10 and 20%) core/active shell UCNPs in cyclohexane using 980 nm laser excitation at 7 W cm^{-2}.

which are predominantly populated by multiple energy transfers from excited Yb^{3+} ions. The Yb^{3+} ions act as a sensitizer for the Tm^{3+} ions due to their relatively high absorption coefficient. From Fig. S5 (ESI†), it is quite clear that the optimum concentration of the Tm^{3+} ion and Yb^{3+} ion in the core is 0.5 and 30 mol%, respectively. The upconversion emission intensities from the $^1D_2$, $^1G_4$ and $^3H_4$ states of Tm^{3+} ions in the core/active shell UCNPs have a similar dependence on the Yb^{3+} concentration, reaching the maximum at the Yb^{3+} concentration of 10% in the shell (Fig. S6, ESI†). The number of photons involved in the energy transfer process (for $NaYF_4$:Yb^{3+}(30)/Tm^{3+}(0.5)@$NaYF_4$:Yb^{3+}(10) core/active shell UCNPs) was estimated by studying the power (*P*) dependence of upconversion emission intensity (*I*) using the relation ($P \propto I^n$, where *n* is the number of photons involved in producing the upconversion emission). The values of *n* obtained from the slope of the log*P* *vs.* log*I* plot (Fig. S7, ESI†) are 3.67, 3.85, 3.0, 2.66 and 2.27, respectively, for the $^1D_2 \rightarrow {}^3H_4$, $^1D_2 \rightarrow {}^3F_4$, $^1G_4 \rightarrow {}^3H_6$, $^1G_4 \rightarrow {}^3F_4$ and $^3H_4 \rightarrow {}^3H_6$ transitions, suggesting the involvement of 4, 4, 3, 3 and 2 photons. Based on the well-known Yb^{3+} sensitized Tm^{3+} upconversion, together with the calculated *n* values, the upconversion mechanism in our samples is illustrated in Fig. S8 (ESI†).

In contrast to the upconversion emission from the $NaYF_4$:Yb^{3+}(30)/Tm^{3+}(0.5)@$NaYF_4$:Yb^{3+}(10) core/active shell UCNPs, a remarkable quenching was observed when Yb^{3+} ions (30 + 10 = 40, in total) were doped into the core UCNPs (Fig. S9, ESI†). This result indicates that incorporation of Yb^{3+} ion only in the shell makes the core/active shell UCNPs efficient to achieve energy transfer upconversion ($Yb^{3+}_{(shell)} \rightarrow Yb^{3+}_{(core)} \rightarrow Tm^{3+}_{(core)}$) *via* a cascade mechanism. Moreover, the core/active shell design can minimize surface quenching induced energy loss and subsequently improve the upconversion emissions. The PXRD and TEM image of the $NaYF_4$:Yb^{3+}(40)/Tm^{3+}(0.5) UCNPs are shown in Fig. S10 (ESI†).

In parallel to upconversion luminescence, we also studied downshifting luminescence from the core and core/active shell UCNPs, which was also found to be dependent on the Yb^{3+} concentration (Fig. S11, ESI†). These results illustrate that the

Yb^{3+} ions in the shell transfer excitation energy to the Yb^{3+} ions in the core, which in turn sensitize the Tm^{3+} ions in the core of the UCNPs.

Optimized upconversion emission intensity at certain Yb^{3+} concentrations (30% in the core and 10% in the shell) is attributed to two concurrent processes. The first one is the harvesting of light, upon 980 nm excitation, by Yb^{3+} ions in the shell and then the transfer of the energy to Yb^{3+} ions in the core. A high concentration of Yb^{3+} ions is expected to increase the upconversion emission due to the increased absorption cross section of the core/active shell UCNPs. The other one is the unfavourable cross relaxation process between the Yb^{3+} ions, which deactivates the harvested energy of Yb^{3+} ions and which even increases with the increase of the Yb^{3+} concentration in both core and shell. A suitable balance between these two processes is achieved only at optimized Yb^{3+} concentrations (10% in the shell and 30% in the core), leading to the most intense signals from the activator (*e.g.* Tm^{3+}). Moreover, $NaYF_4$:Tm^{3+}(0.5)/Yb^{3+}(30) not only acts as a superior core but also favours intense upconversion emission from Tm^{3+} ions. This facilitates the $Yb^{3+}_{(shell)} \rightarrow Yb^{3+}_{(core)}$ energy transfer process. The efficiency of a nonradiative energy transfer can be quantified using the following equation:

$$ET = 1 - I_{DA}/I_D$$

where ET stands for energy transfer efficiency, and I_{DA} and I_D are the upconversion emission intensity of the energy donor in the presence and absence of an energy acceptor, respectively. Following this equation, the energy transfer efficiency was determined to be ~90% and ~40% for the $NaYF_4$:Yb^{3+}(30)/Tm^{3+}(0.5)@$NaYF_4$:Yb^{3+}(10) and $NaYF_4$:Yb^{3+}(40)/Tm^{3+}(0.5)@$NaYF_4$(0) UCNPs containing 10% and 0% Yb^{3+} ions in the shell, respectively. These results confirm the importance of using a 30% Yb^{3+} enriched $NaYF_4$ host lattice as a core and 10% Yb^{3+} enriched $NaYF_4$ as a shell to produce efficient $Yb^{3+}_{(shell)} \rightarrow Yb^{3+}_{(core)}$ energy transfer.

To integrate the core and core/active shell UCNPs with water dispersible NIR-II (IR-1061) dye, an oleic acid ligand on the surface of the UCNPs was firstly replaced by the positively charged polyethyleneimine (PEI) ligand. Replacement of oleic acid and further capping of PEI ligand onto the surface of the core and core/active shell UCNPs were confirmed by the absence and presence of vibrational modes of –COOH and $–NH_2$ (along with –CN and –NH) groups, respectively (Fig. S12, ESI†). After HCl treatment, the aqueous dispersion of UCNPs becomes acidic and the zeta potential value of bare UCNPs is found to be +47.3 mV. With an increase in pH, the zeta potential value also starts to decrease,[52] making the surface feasible for binding with the PEI ligand, which is positively charged. PEI-capped water-dispersible UCNPs possess a +31.3 mV zeta potential value. Upon ligand exchange, there is hardly any change in the crystalline phase (Fig. S13, ESI†) and size (Fig. 3) of the core/active shell UCNPs observed. Moreover, we calculated the upconversion emission for the water-dispersible core and core/active shell UCNPs. Fig. 4 clearly depicts that the core/active shell UCNPs having 10% Yb^{3+} in the shell exhibit the strongest luminescence. The trend in upconversion emission from the water-dispersible core/active shell UCNPs is similar to that of the oleic acid coated UCNPs except for a slight decrease in emission intensity.

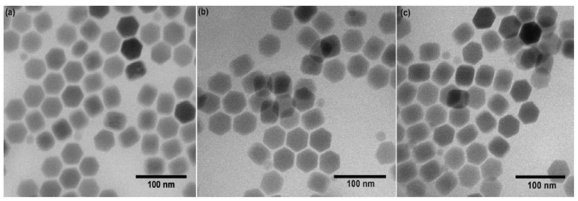

Fig. 3 TEM images of PEI-capped $NaYF_4$:Yb^{3+}(30)/Tm^{3+}(0.5)@$NaYF_4$:Yb^{3+}(*X*) core/active shell UCNPs where *X* = 0, 5 and 10% in a, b and c, respectively.

On the other hand, water-dispersible IR-1061 dye was synthesized using tip sonication *via* a phase transfer process. Encapsulation with Pluronic F68 poloxamer renders the dye water-dispersible because of the (−)ve charge of the –OH groups. The zeta potential value of Pluronic F68 encapsulated IR-1061 dye was found to be (−) 10.9 mV. The zeta potential graphs of PEI capped $NaYF_4$:Yb^{3+}(30)/Tm^{3+}(0.5)@$NaYF_4$:Yb^{3+}(10) core/active shell UCNPs and Pluronic F68 encapsulated IR-1061 dye are shown in Fig. S14 (ESI†).

The characteristic absorption spectra of the dye in pure form and in water-dispersible form are shown in Fig. 5. It is clear from the spectra that the water-dispersible dye has a much broader absorption in water than in bare or pristine form dissolved in dichloromethane (DCM). Moreover, it is interesting to note that both 808 and 980 nm laser excitation points are lying in the broad range absorption of the dye in water. Thus, the water dispersible dye could be excited using both laser excitations. This assumption is further supported by the photoluminescence (PL) emission measurement of dye in water. Upon 808 and 980 nm laser excitations, the dye molecule shows a similar PL character (Fig. S15, ESI†), suggesting the plausibility of dye excitation using both lasers. It is worth mentioning that 808 nm laser excitation is better than 980 nm laser excitation for biological applications as using 980 nm laser excitation also leads to unwanted overheating, which is harmful for biological species. Moreover, as mentioned

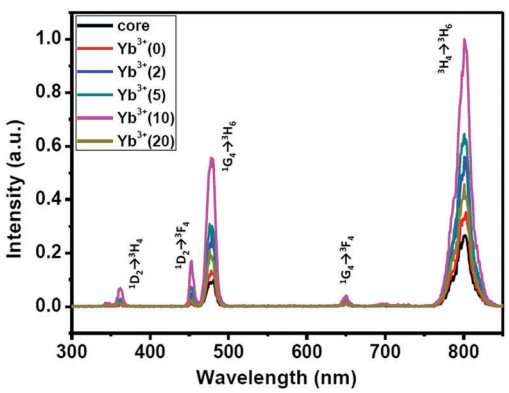

Fig. 4 Upconversion emission spectra of PEI-capped $NaYF_4$:$NaYF_4$:Yb^{3+}(30)/Tm^{3+}(0.5) core and $NaYF_4$:$NaYF_4$:Yb^{3+}(30)/Tm^{3+}(0.5)@$NaYF_4$:Yb^{3+}(*X*) (*X* = 0, 2, 5, 10, 20%) core/active shell UCNPs in water using 980 nm laser excitation at 7 W cm^{-2}.

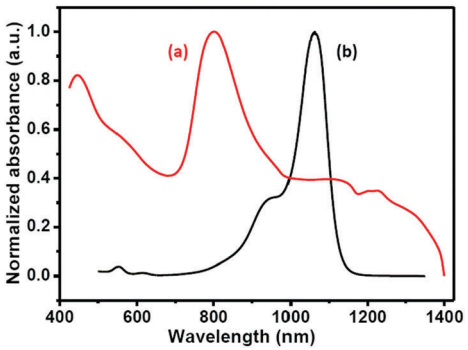

Fig. 5 Absorption spectra of (a) Pluronic F68-encapsulated IR-1061 dye in water and (b) pure IR-1061 dye in DCM.

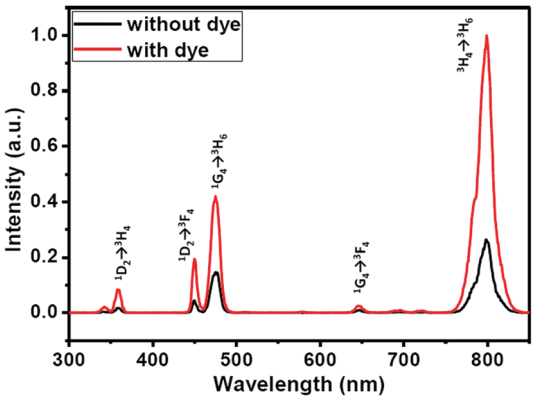

Fig. 6 Upconversion emission spectra of $NaYF_4$:Yb^{3+}(30)/Tm^{3+}(0.5%)@$NaYF_4$:Yb^{3+}(10) core/active shell UCNPs with and without dye sensitization.

earlier, our main goal was to achieve strong NIR-I (*i.e.* ~800 nm from Tm^{3+} ion) emission, which might be lost if the same wavelength (808 nm) is used for excitation. Furthermore, the upconversion emission from the UCNPs overlaps with the absorption of water dispersible IR-1061 dye in the 800 nm region (Fig. S16, ESI†), which is not good for sensitization experiments as the dye should be highly transparent to the upconverted photons emitted by the core/active shell UCNPs.

The emission spectrum of water-dispersible NIR-1061 dye overlaps with the absorption peak of the Yb^{3+} ions of the $NaYF_4$:Yb^{3+}(30)/Tm^{3+}(0.5)@$NaYF_4$:Yb^{3+}(10) core/active shell UCNPs (Fig. S17, ESI†). Though this overlap is not very strong, the high absorption capability of the dye molecules allows the nonradiative energy transfer from water-dispersible NIR-1061 dye to Yb^{3+} ions in the shell and consequently to Yb^{3+} ions in the core.

A short distance between UCNPs and dye is essential for efficient energy transfer between them. The interaction of the water-dispersible NIR-1061 dye with the UCNP surface is a complex process that might involve electrostatic interaction or physical adsorption or even covalent conjugation. Among all these complex processes, electrostatic interaction occurs only when the UCNPs (acceptor) and dye (donor) carry opposite charges on their surface. In accordance with our earlier discussions, our UCNPs and dye meet these criteria. After efficient electrostatic interaction, the zeta potential value of PEI capped UCNPs decreases from (+) 31.3 mV to (+) 23 mV. The average size of the PEI-coated UCNPs increases from 44 ± 2.4 nm to 51 ± 3.1 nm after electrostatic coupling with the water-dispersible dye (Fig. S18, ESI†). This small increase may be related to the partial aggregation of the UCNPs.

To further verify this, a control experiment was performed. The absorption maximum wavelength of NIR-1061 dye undergoes a blue shift from 801 nm to 797 nm when combined with the core/active shell UCNPs (Fig. S19, ESI†). However, the orientation of the dye molecules on the surface of the UCNPs is not still clear.

We examined the upconversion emission for the water-dispersible $NaYF_4$:Yb^{3+}(30)/Tm^{3+}(0.5)@$NaYF_4$:Yb^{3+}(10) core/active shell UCNPs with water-dispersible IR-1061 dye sensitization under 980 nm laser excitation. Fig. 6 compares the upconversion luminescence from the $NaYF_4$:Yb^{3+}(30)/Tm^{3+}(0.5%)@$NaYF_4$:Yb^{3+}(10) core/active shell UCNPs with and without dye sensitization. Upon addition of 0.6 μM dye to the UCNP dispersion (0.01 μM), 283% enhancement (3.8 time) in the NIR signal (~800 nm emission from Tm^{3+} ion) was observed (Fig. 6). Upconversion luminescence from other states of Tm^{3+} ions is also observed to increase to different extents. (Fig. S20, ESI†). Similar trends were observed in the case of the core particles and other core/active shell UCNPs prepared with different amounts of Yb^{3+} in the shell (Fig. 7). Interestingly, a twist in the results comes when the core and core/shell having no Yb^{3+} in the shell are compared. The increase in the NIR-I signal for the core becomes higher than that of the core/shell having 0% Yb^{3+} in the shell. Thus, the inert shell having no Yb^{3+} ion has an adverse effect on the dye sensitization process. The integrated area of the upconversion emission peak (800 nm) for the dye-sensitized $NaYF_4$:Yb^{3+}(30)/Tm^{3+}(0.5%)@$NaYF_4$:Yb^{3+}(10) core/active shell UCNPs was 2.87 times higher than the dye-sensitized core UCNPs ($NaYF_4$:Yb^{3+}(30)/Tm^{3+}(0.5)) and 3.32 times higher than the same sized dye-sensitized $NaYF_4$:Yb^{3+}(30)/Tm^{3+}(0.5%)@$NaYF_4$:Yb^{3+}(0) UCNPs. In this study, we also increased the Yb^{3+} content to 20% in the shell layer and found that above the optimal doping concentration (10% Yb^{3+}), the upconversion emission intensity decreases (Fig. 7). This decrease is presumably caused by Yb^{3+} cross relaxation quenching. Moreover,

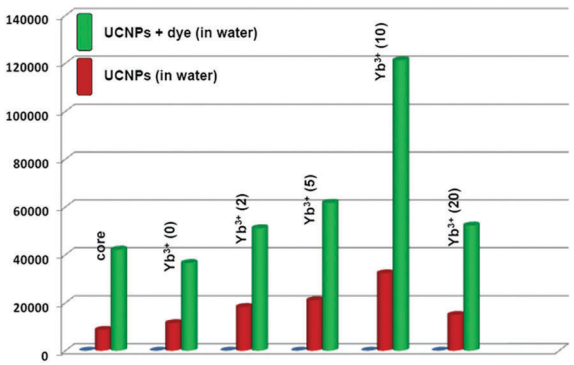

Fig. 7 Bar diagram indicating enhancement in NIR-I (~800 nm) emission from water-dispersible NIR-II dye-sensitized UCNPs (both core and core/shell with different amounts of Yb^{3+} ions in shell) in water (λ_{ex} = 980 nm laser, 7 W cm^{-2}).

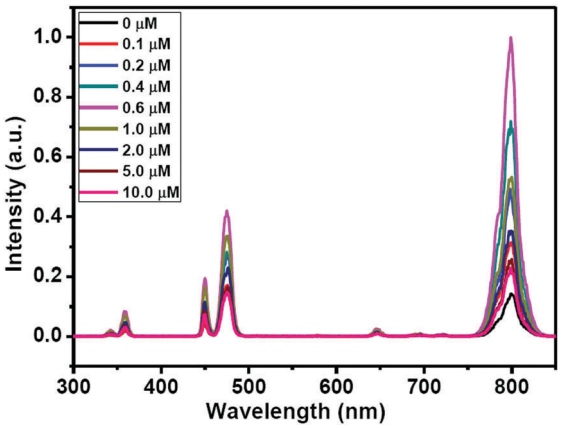

Fig. 8 Upconversion emission of water dispersible $NaYF_4$:Tm^{3+}(0.5)/Yb^{3+}(30)@$NaYF_4$:Yb^{3+}(10) UCNP suspension (0.01 μM) against different concentrations of dye in water (λ_{ex} = 980 nm laser, 7 W cm^{-2}).

another control experiment with $NaYF_4$:Yb^{3+}(40)/Tm^{3+}(0.5) core UCNPs (~27 nm) was also carried out. Upon 980 nm laser excitation, the upconversion emission intensity of the water-dispersible IR-1061 dye-sensitized $NaYF_4$:Yb^{3+}(40)/Tm^{3+}(0.5) core UCNPs was also much lower than that of the $NaYF_4$:Yb^{3+}(30)/Tm^{3+}(0.5%)@$NaYF_4$:Yb^{3+}(10) core/active shell UCNPs (Fig. S21, ESI†).

To find the optimal ratio between the water-dispersible dye and core/active shell UCNPs and thus get an intense NIR-I signal, we added different concentrations of dye to the $NaYF_4$:Yb^{3+}(30)/Tm^{3+}(0.5%)@$NaYF_4$:Yb^{3+}(10) core/active shell UCNP dispersion (fixed concentration of 0.01 μM) (Fig. 8). A gradual increase in the upconversion emission intensity of all emissions from Tm^{3+} ions is noticed with an increase in the dye concentration up to 0.6 μM. Further increasing the dye concentration led to a decrease in upconversion emission intensity. The adverse effect of high dye loading (>0.6 μM) can be explained considering two factors: (i) increased mutual interactions between the water-dispersible dye on the core/active shell UCNP surface (*i.e.* self-quenching) and (ii) an increased concentration of non-interacting (excess) dye molecules that absorb the excitation energy but do not transfer it to the UCNPs.

To get proof for the optimal ratio between the water-dispersible dye and core/active shell UCNPs in a reverse way, we added different concentrations of UCNPs to the dye dispersion, where dye concentration was fixed at 0.6 μM. Upon addition of 0.01 μM UCNPs, the PL emission intensity of the dye was found to decrease (Fig. S22, ESI†). These results clearly indicate that for efficient energy transfer between the water-dispersible IR-1061 dye and UCNPs, the optimal ratio is UCNPs : dye = 1 : 60. Calculation of the approximate concentration of core/active shell UCNPs in water is shown in Section SC in the ESI.†

Furthermore, we carried out the photostability study of the water-dispersible IR-1061 dye and water-dispersible IR-1061 dye-sensitized $NaYF_4$:Yb^{3+}(30)/Tm^{3+}(0.5%)@$NaYF_4$:Yb^{3+}(10) core/active shell UCNPs. The nature of the absorption spectra remains almost unchanged except for a slight decrease in the absorbance value (Fig. S23, ESI†). These results suggest that the antenna effect is only generated by the water-dispersible IR-1061 dye interacting with the core/active shell UCNP surface. We further studied the stability of the prepared water-dispersible IR-1061 dye-sensitized $NaYF_4$:Yb^{3+}(30)/Tm^{3+}(0.5%)@$NaYF_4$:Yb^{3+}(10) core/active shell UCNPs by measuring the upconversion emission spectrum of the same as a function of time under 980 nm laser excitation. From Fig. S24 (ESI†), it is clearly noted that after as long as 10 h, the upconversion emission intensity decreases by only around 40%, indicating the reasonable stability of the water-dispersible dye-sensitized UCNPs. There is, however, room for further improvement of the stability through a closer contact between dye and UCNPs, possibly *via* strong electrostatic interaction.

The dye antenna effect may occur through a radiative or nonradiative path. Upon dilution, the upconversion emission intensity of the water-dispersible IR-1061 dye-sensitized $NaYF_4$:Yb^{3+}(30)/Tm^{3+}(0.5%)@$NaYF_4$:Yb^{3+}(10) core/active shell UCNPs decreases gradually (Fig. 9) and the plot of change in upconversion emission intensity against concentration becomes linear (Fig. S25, ESI†). This result rules out the possibility of any radiative type energy transfer mechanism. Moreover, we measured the decay of emission of the $^1G_4$ state (concerning $^1G_4 \rightarrow {}^3H_6$ transition) of the Tm^{3+} ion of the core/active shell UCNPs and dye-sensitized core/active shell UCNPs. From Fig. S26 (ESI†), it is quite clear that the average lifetime of the $^1G_4$ sate of the Tm^{3+} ion increases from ~60 μs (for core/active shell UCNPs) to ~105 μs (for dye-sensitized core/active shell UCNPs, [dye] = 0.6 μM). This increase in emission lifetime again confirms a non-radiative type energy transfer mechanism from dye to UCNPs.

The maximal efficiency of nonradiative energy transfer was determined to be ~30% for the optimized core/active shell UCNPs doped with 10% Yb^{3+} in the shell. The energy transfer efficiency (E) is calculated using $1 - (I_{DA}/I_D)$, where I_{DA} and I_D represent the emission intensity from water-dispersible NIR-1061 dye in the presence and absence of the acceptor (UCNPs), respectively. The nonradiative energy transfer from water-dispersible IR-1061 dye to Yb^{3+} ions (in core/active shell UCNPs) might take place through either Föster type or Dexter type mechanisms. We presume that the Föster type is more likely to occur in our case. The short distance between the water-dispersible IR-1061 dye and the Yb^{3+} ions (in the shell) as well as the random distribution of the Yb^{3+} ions in a 5.5 nm thick shell support the above assumption, though the energy gap

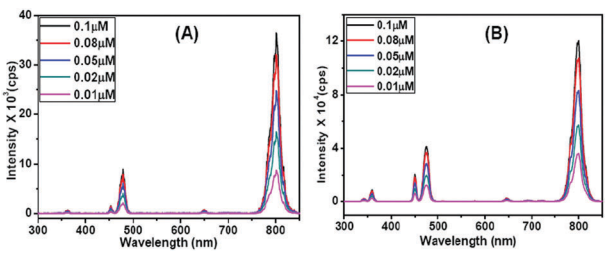

Fig. 9 Upconversion emission spectra of (A) $NaYF_4$:Yb^{3+}(30)/Tm^{3+}(0.5%)@$NaYF_4$:Yb^{3+}(0) and (B) $NaYF_4$:Yb^{3+}(30)/Tm^{3+}(0.5%)@$NaYF_4$:Yb^{3+}(10) core/active shell UCNPs against dilution of the same.

between dye and Yb^{3+} ions is not clear to us. To understand the efficient energy transfer process between the water-dispersible dye and core/active shell UCNPs, we calculated the Föster distance R_0 between them, where R_0 is the distance between the donor and acceptor at which energy transfer efficiency is 50% between the two. It is calculated using the following equation:

$$R_0 = 0.211\left[\frac{\kappa^2 \Phi_D J(\lambda)}{\eta^4}\right]^{1/6}$$

where κ is an orientation factor between the donor and acceptor (κ^2 = 2/3), η refers to the refractive index, Φ_D is the fluorescence quantum yield (Section SD in the ESI†) of the donor (water-dispersible dye) in the absence of the acceptor and $J(\lambda)$, in units of M^{-1} cm^{-1} nm^4, is the overlap integral between the normalized emission spectrum of the donor and the absorption spectrum of the acceptor (core/active shell UCNPs). J is defined by the equation as follows:

$$J(\lambda) = \int_0^\infty F_D(\lambda)\varepsilon_A(\lambda)\lambda^4 d\lambda$$

where ε_A is the extinction coefficient of the acceptor in units of M^{-1} cm^{-1}, λ is the wavelength in nm and F_D is the wavelength dependent donor emission spectrum normalized to an area of numeric 1. The obtained $J(\lambda)$ value for the donor acceptor pair was found to be 1.59×10^{17} M^{-1} cm^{-1} nm^4. This value was then used to calculate the Föster distance (R_0), which was found to be 33.38 Å. The energy transfer efficiency (E) between the water dispersible dye and core/active shell UCNPs was calculated to be ~30%. These values were then used to calculate the average distance (r) between the donor and acceptor following the equation:

$$r = R_0[(1/E) - 1]^{1/6}$$

The average distance (r) between the donor and acceptor was found to be 38.44 Å. Moreover, the average intermolecular distance of the water-dispersible IR-1061 dye on the surface of the core/active shell UCNPs (Section SE, in the ESI†) was determined to be 8.7 nm at optimal dye concentration. Finally, the upconversion quantum efficiency (UQE) of the water-dispersible IR-1061 dye sensitized core/active shell UCNPs was evaluated to be 6.1%, when excited at 980 nm laser with a power density of 7 W cm^{-2}. This UQE value is lower than the recent literature reports based on IR-808 or IR-806 dye sensitized core/active shell UCNPs wherein sensitization experiments were carried out in non-water solvent.[48,49] The calculation of quantum efficiency for the $NaYF_4$:Yb^{3+}(30)/Tm^{3+}(0.5%)@$NaYF_4$:Yb^{3+}(10) core/active shell UCNPs is shown in Section SF in the ESI.†

Conclusions

We propose, for the first time, the use of a water-dispersible NIR-II dye (IR-1061) with a broader absorption in aqueous medium to sensitize $NaYF_4$:Yb^{3+}(30)/Tm^{3+}(0.5%)@$NaYF_4$:Yb^{3+} core/active shell UCNPs and improve their upconversion efficiency. Instead of the native form of the dye commonly employed in dye-sensitization studies in non-aqueous media, the proposed water-dispersible and Pluronic F68-encapsulated dye (IR-1061) is able to effectively harvest irradiation energy when conjugated with polyethyleneimine (PEI) coated-$NaYF_4$:Tm^{3+}/Yb^{3+}@$NaYF_4$:Yb^{3+} core/active shell UCNPs. This harvested energy is nonradiatively transferred to the Yb^{3+} ions in the shell and subsequently to the Yb^{3+} ions in the core that sensitize Tm^{3+} ions positioned in the core to generate upconversion emission from the core/active shell UCNPs. We achieved around 283% enhancement in NIR-I emission (800 nm emission of the Tm^{3+} ion) from the water-dispersible IR-1061-sensitized core/active shell UCNPs *via* doping of ytterbium ions (Yb^{3+}, 10% optimal) in the UCNP shell. We have carried out a detailed characterization of the proposed dye/UCNP system, highlighting the possible energy transfer mechanism as well as the effect of the shell and core configuration and dye-loading on the upconversion response of the system. We thus offer an interesting strategy to improve NIR-I emission from core/active shell UCNPs, which will pave the way for new biological and medical applications.

Conflicts of interest

The authors have no competing and/or relevant financial interest(s) to disclose.

Acknowledgements

The authors acknowledge Brazilian agencies CNPq, CAPES and FAPESP for financial support. C. Hazra and S. Ullah acknowledge financial support from the São Paulo Research Foundation (FAPESP, Brazil) under fellowship grant number 2015/18733-0 and 2015/22875-4, respectively. Y. E. S. Correales thanks CNPq for the master degree fellowship (Grant no. 133105/2017-2).

Notes and references

1 M. Haase and H. Schäfer, *Angew. Chem., Int. Ed.*, 2011, **50**, 5808–5829.
2 C. Dong and F. C. J. M. van Veggel, *ACS Nano*, 2009, **3**, 123–130.
3 F. Wang, Y. Han, C. S. Lim, Y. Lu, J. Wang, J. Xu, H. Chen, C. Zhang, M. Hong and X. Liu, *Nature*, 2010, **463**, 1061–1065.
4 J. Pichaandi, J. C. Boyer, K. R. Delaney and F. C. J. M. van Veggel, *J. Phys. Chem.*, 2011, **115**, 19054–19064.
5 V. Mahalingam, R. Naccache, F. Vetrone and J. A. Capobianco, *Chem. Commun.*, 2011, **47**, 3481–3483.
6 S. Ullah, C. Hazra, E. P. Ferreira-Neto, T. C. Silva, U. P. R. Rodrigues-Filho and S. J. L. Ribeiro, *CrystEngComm*, 2017, **19**, 3465–3475.
7 W. Shao, G. Chen, A. Kuzmin, H. L. Kutscher, A. Pliss, T. Y. Ohulchanskyy and P. N. Prasad, *J. Am. Chem. Soc.*, 2016, **138**, 16192–16195.
8 Z. Li, Y. Zhang, H. La, R. Zhu, G. El-Banna, Y. Wei and G. Han, *Nanomaterials*, 2015, **5**, 2148–2168.

9 J. Zhang, Y. Huang, L. Jin, F. Rosei, F. Vetrone and J. P. Claverie, *ACS Appl. Mater. Interfaces*, 2017, **9**, 8142–8150.
10 C. D. S. Brites, X. Xie, M. L. Debasu, X. Qin, R. Chen, W. Huang, J. Rocha, X. Liu and L. D. Carlos, *Nat. Nanotechnol.*, 2016, **11**, 851–856.
11 Y. Zhang, Z. Yu, J. Li, Y. Ao, J. Xue, Z. Zeng, X. Yang and T. T. Y. Tan, *ACS Nano*, 2017, **11**, 2846–2857.
12 Chengli Wang, Xiaomin Li and Fan Zhang, *Analyst*, 2016, **141**, 3601–3620.
13 P. Alonso-Cristobal, P. Vilela, A. El-Sagheer, E. Lopez-Cabarcos, T. Brown, O. L. Muskens, J. Rubio-Retama and A. G. Kanaras, *ACS Appl. Mater. Interfaces*, 2015, **7**, 12422–12429.
14 S. Hao, G. Chen and C. Yang, *Theranostics*, 2013, **3**, 331–345.
15 S. Xu, B. Dong, D. Zhou, Z. Yin, S. Cui, W. Xu, B. Chen and H. Song, *Sci. Rep.*, 2016, **6**, 23406.
16 K. Nigoghossian, S. Ouellet, J. Plain, Y. Messaddeq, D. Boudreau and S. J. L. Ribeiro, *J. Mater. Chem. B*, 2017, **5**, 7109–7117.
17 G. Jalani, R. Naccache, D. H. Rosenzweig, L. Haglund, F. Vetrone and M. Cerruti, *J. Am. Chem. Soc.*, 2016, **138**, 1078–1083.
18 F. Wang, D. Banerjee, Y. Liu, X. Chen and X. Liu, *Analyst*, 2010, **135**, 1839–1854.
19 G. E. Arnaoutakis, J. Marques-Hueso, A. Ivaturi, S. Fischer, J. C. Goldschmidt, K. W. Krämer and B. S. Richards, *Sol. Energy Mater. Sol. Cells*, 2015, **140**, 217–223.
20 S. Hao, Y. Shang, D. Li, H. Ågren, C. Yang and G. Chen, *Nanoscale*, 2017, **9**, 6711–6715.
21 C. Yuan, G. Chen, L. Li, J. A. Damasco, Z. Ning, H. Xing, T. Zhang, L. Sun, H. Zeng, A. N. Cartwright, P. N. Prasad and H. Ågren, *ACS Appl. Mater. Interfaces*, 2014, **6**, 18018–18025.
22 B. Zhou, B. Shi, D. Jin and X. Liu, *Nat. Nanotechnol.*, 2015, **10**, 924–936.
23 R. Deng, F. Qin, R. Chen, W. Huang, M. Hong and X. Liu, *Nat. Nanotechnol.*, 2015, **10**, 237–242.
24 B. M. van der Ende, L. Aarts and A. Meijerink, *Adv. Mater.*, 2009, **21**, 3073–3077.
25 Y. G. Chen, H. L. Qju, P. N. Prasad and X. Y. Chen, *Chem. Rev.*, 2014, **114**, 5161–5214.
26 J.-C. G. Bünzli, *Chem. Rev.*, 2010, **110**, 2729–2755.
27 C. R. Ronda, T. Jüstel and H. Nikol, *J. Alloys Compd.*, 1998, **275-277**, 669–676.
28 S. V. Eliseeva and J. C. G. Bünzli, *New J. Chem.*, 2011, **35**, 1165–1176.
29 S. V. Eliseeva and J. C. G. Bünzli, *Chem. Soc. Rev.*, 2010, **39**, 189–227.
30 K. Nigoghossian, Y. Messaddeq, D. Boudreau and S. J. L. Ribeiro, *ACS Omega*, 2017, **2**, 2065–2071.
31 V. Fernandez-Moreira, B. Song, V. Sivagnanam, A.-S. Chauvin, C. D. B. Vandevyver, M. A. M. Gijs, I. A. Hemmila, H.-A. Lehr and J.-C. G. Bünzli, *Analyst*, 2010, **135**, 42–52.
32 Z. Q. Li and Y. Zhang, *Nanotechnology*, 2008, **19**, 5.
33 F. Wang, Y. Han, C. S. Lim, Y. H. Lu, J. Wang, J. Xu, H. Y. Chen, C. Zhang, M. H. Hong and X. G. Liu, *Nature*, 2010, **463**, 1061–1065.
34 R. R. Deng, F. Qin, R. F. Chen, W. Huang, M. H. Hong and X. G. Liu, *Nat. Nanotechnol.*, 2015, **10**, 237–242.
35 C. G. Bünzli, *Chem. Rev.*, 2002, **102**, 1897–1928.
36 G. Blasse and B. C. Grabmaier, *Luminescent Materials*, Springer, Berlin, 1994.
37 D. M. Wu, A. Garcia-Etxarri, A. Salleo and J. A. Dionne, *J. Phys. Chem. Lett.*, 2014, **5**, 4020–4031.
38 M. Saboktakim, X. Ye, U. K. Chettiar, N. Engheta, C. B. Murray and C. R. Kagan, *ACS Nano*, 2013, **7**, 7186–7192.
39 F. Vetrone, R. Naccache, V. Mahalingam, C. G. Morgan and J. A. Capobianco, *Adv. Funct. Mater.*, 2009, **19**, 2924–2929.
40 S. Hao, G. Chen, C. Yang, W. Shao, W. Wei, Y. Liu and P. N. Prasad, *Nanoscale*, 2017, **9**, 10633–10638.
41 X. M. Li, R. Wang, F. Zhang and D. Y. Zhao, *Nano Lett.*, 2014, **14**, 3634–3639.
42 N. J. J. Johnson, S. He, S. Diao, E. M. Chan, H. Dai and A. Almutairi, *J. Am. Chem. Soc.*, 2017, **139**, 3275–3282.
43 J. B. Zhao, D. Y. Jin, E. P. Schartner, Y. Q. Lu, Y. J. Liu, A. V. Zvyagin, L. X. Zhang, J. M. Dawes, P. Xi, J. A. Piper, E. M. Goldys and T. M. Monro, *Nat. Nanotechnol.*, 2013, **8**, 729–734.
44 J. Schmidt and A. Penzkofer, *J. Chem. Phys.*, 1989, **91**, 1403–1409.
45 L. D. Deloach, S. A. Payne, L. L. Chase, L. K. Smith, W. L. Kway and W. F. Krupke, *IEEE J. Quantum Electron.*, 1993, **29**, 1179–1191.
46 W. Zou, C. Visser, J. A. Maduro, M. S. Pshenichnikov and J. C. Hummelen, *Nat. Photonics*, 2012, **6**, 560–564.
47 G. Y. Chen, H. Agren, T. Y. Ohulchanskyy and P. N. Prasad, *Chem. Soc. Rev.*, 2015, **44**, 1680–1713.
48 G. Chen, J. Damasco, H. Qiu, W. Shao, T. Y. Ohulchanskyy, R. R. Valiev, X. Wu, G. Han, Y. Wang, C. Yang, H. Ågren and P. N. Prasad, *Nano Lett.*, 2015, **15**, 7400–7407.
49 X. Wu, Y. Zhang, K. Takle, O. Bilsel, Z. Li, H. Lee, Z. Zhang, D. Li, W. Fan, C. Duan, E. M. Chan, C. Lois, Y. Xiang and G. Han, *ACS Nano*, 2016, **10**, 1060–1066.
50 J. Xu, P. Yang, M. Sun, H. Bi, B. Liu, D. Yang, S. Gai, F. He and J. Lin, *ACS Nano*, 2017, **11**, 4133–4144.
51 F. Wang, R. Deng and X. Liu, *Nat. Protoc.*, 2014, **9**, 1634–1644.
52 N. Bogdan, F. Vetrone, G. A. Ozin and J. A. Capobianco, *Nano Lett.*, 2011, **11**, 835–840.